Conformal boundary loop models

Jesper Jacobsen, Hubert Saleur

Conformal boundary loop models

Jesper Lykke Jacobsen[1,2] and Hubert Saleur[2,3]

[1] LPTMS, Université Paris-Sud, Bâtiment 100,
Orsay, 91405, France
[2] Service de Physique Théorique, CEA Saclay,
Gif Sur Yvette, 91191, France
[3] Department of Physics and Astronomy, University of Southern California,
Los Angeles, CA 90089, USA

September 17, 2007

Abstract

We study a model of densely packed self-avoiding loops on the annulus, related to the Temperley Lieb algebra with an extra idempotent boundary generator. Four different weights are given to the loops, depending on their homotopy class and whether they touch the outer rim of the annulus. When the weight of a contractible bulk loop $x \equiv q + q^{-1} \in (-2, 2]$, this model is conformally invariant for any real weight of the remaining three parameters. We classify the conformal boundary conditions and give exact expressions for the corresponding boundary scaling dimensions. The amplitudes with which the sectors with any prescribed number and types of non contractible loops appear in the full partition function Z are computed rigorously. Based on this, we write a number of identities involving Z which hold true for any finite size. When the weight of a contractible boundary loop y takes certain discrete values, $y_r \equiv \frac{[r+1]_q}{[r]_q}$ with r integer, other identities involving the standard characters $K_{r,s}$ of the Virasoro algebra are established. The connection with Dirichlet and Neumann boundary conditions in the $O(n)$ model is discussed in detail, and new scaling dimensions are derived. When q is a root of unity and $y = y_r$, exact connections with the A_m type RSOS model are made. These involve precise relations between the spectra of the loop and RSOS model transfer matrices, valid in finite size. Finally, the results where $y = y_r$ are related to the theory of Temperley Lieb cabling.

SPhT-T06/155

1 Introduction

Boundary conformal field theories (CFT) have lately played an increasingly important role in statistical mechanics, condensed matter physics and string theory. In statistical mechanics, they appear in most probabilistic applications of geometrical models (see, e.g., [1] for a recent example), in particular through SLE [2]. In condensed matter, they contain all the information about fixed points in theories which are gapless in the bulk, such as Kondo systems or edge states in the fractional quantum Hall effect (see [3] for a review). In string theory, they provide for instance microscopic techniques to study D-branes in curved backgrounds [4]. On top of this, the study of boundary aspects is a crucial component of understanding and classifying CFTs at large [5], and has lately played a crucial role in the solution of non rational CFTs [6].

While progress in understanding conformal boundary conditions for rational CFTs has been considerable, the situation is not so satisfactory for non rational theories, which are however all too frequent in statistical mechanics applications. A case in point concerns the loop or cluster models, which—in one guise or another—are hidden behind most simple models of interest, such as Q-state Potts models,

$O(n)$ models, RSOS models, polymers, and percolation. We are not aware of answers to most questions one might ask in this context, such as "what are all the conformal invariant boundary conditions", or "what are the partition functions for the $O(n)$ models with Neumann boundary conditions", etc. The origin of this difficulty lies in our lack of understanding of the bulk CFTs, which exhibit non-rational, logarithmic features, and for which too little is known. Bulk exponents turned out to be tractable thanks to the Coulomb gas technique, but this technique has not been generalized to the boundary case with sufficient control yet (see [1] for recent progress in this direction).

We put forward in this paper a proposal for what we believe are all the conformal boundary conditions of dense loop models. For each of those we determine the critical exponents, operator content and boundary partition functions, some of which have interesting probabilistic or geometrical interpretations.

There seems to be much substance behind the results we uncover, and we hope to get back to the question in more details in the near future. In the present paper, we only present the leading arguments—which are based on previously published but unexploited results, as well as algebraic considerations—together with intensive numerical checks and some combinatorial proofs.

To help the reader, we now give a quick summary of our results and notations. The *boundary loop model* (BLM) to be studied is defined on a tilted square lattice (see Fig. 3), wrapped on an annulus of width N strands and circumference M lattice spacings. Loops cover all the edges, and interact in a specific way with the outer rim of the annulus, whereas they are simply reflected by the inner rim (free boundary conditions). We denote by L the number of non contractible loops (note that L and N must have the same parity). Any loop has one of four weights (x, y, l or m, see Fig. 8): l (resp. m) for a non contractible loop never touching (resp. touching at least once) the outer rim, and similarly x (resp. y) for contractible loops. We parametrize $x = q + q^{-1} \in (-2, 2]$ by $q = \mathrm{e}^{i\pi/(p+1)}$ (p real); the model is then critical with central charge (2.7) for any real values of y, l, m and is endowed with the $U_q(sl_2)$ quantum group symmetry. We further parametrize $y = y(r)$ as in (2.4). Our central claim is that for any *real* r, and any L, there are two (distinct for $L > 0$) conformal boundary conditions: *blobbed* (resp. *unblobbed*) in which the outermost non contractible loop is required to (resp. required not to) touch the outer rim of the annulus. (When $L = 0$ the two cases coincide.) The spectrum generating functions in these two cases are (3.8), and the boundary conformal weights (critical exponents) $h_{r,r\pm L}$ are read off from (2.8). They combine to form the BLM partition function Z through the amplitudes (3.11). When $p \geq 1$ is integer, and when further $r = 1, 2, \ldots, p$ the BLM model can be related to an RSOS model of the A_p type with specific boundary conditions (three columns of fixed heights, see Fig. 12) through the rules (4.4). In the latter case, Z can be written as a sum (3.18) over irreducible representations of the Virasoro algebra.

The paper is organized as follows. In Section 2 we review the algebraic framework used in our study (the blob algebra) along with a few key results. In Section 3 we define the BLM, classify its conformal boundary conditions, and give exact results for the associated critical exponents. Two appendices present a rigorous result on the amplitudes of the transfer matrix eigenvalues. This is used in Section 3.4 to write a number of exact identities—exact in finite size—relating Z to Virasoro characters $K_{r,s}$. In Section 3.5 we discuss the case of Neumann boundary conditions for the loop model, identifying in particular the Neumann to Dirichlet boundary condition changing field. The relations to RSOS models are discussed in Section 4. Finally, in Section 5, we comment on the relation between the blob algebra and the theory of Temperley Lieb cabling. Our conclusions—and the prospects for (much) further work—are given in Section 6.

2 The blob algebra

The Temperley Lieb (TL) algebra $\mathcal{T}_N(x)$ on N strands is defined by the generators e_i ($i = 1, 2, \ldots, N-1$) acting on strands i and $i+1$ and satisfying the well-known relations

$$\begin{aligned} e_i e_j &= e_j e_i \text{ for } |i-j| \geq 2 \\ e_i e_{i\pm 1} e_i &= e_i \\ e_i^2 &= x e_i \end{aligned} \tag{2.1}$$

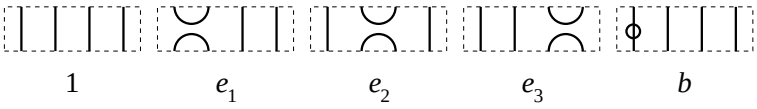

Figure 1: Graphical representation of the action of the generators of the blob algebra, here shown for a system of $N = 4$ strands.

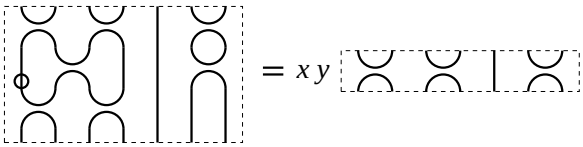

Figure 2: The word $e_1e_3e_6e_2e_6be_1e_3 = xye_1e_3e_6$ in the blob algebra $\mathcal{B}(x, y)$ on $N = 7$ strands.

In [7] this was generalized into the two parameter "blob algebra" $\mathcal{B}_N(x, y)$, having an extra generator b, and satisfying in addition the relations

$$\begin{aligned} b^2 &= b \\ e_1be_1 &= ye_1 \\ e_ib &= be_i \quad \text{for } i = 2, 3, \ldots, N-1 \end{aligned} \tag{2.2}$$

For $\mathcal{T}_N(x)$ it is well-known how to interpret these algebraic relations graphically in terms of the strands. The extra generator b marks the leftmost strand by adding a "blob" to it (see Figure 1). In this graphical representation any completed loop may be taken out and replaced by its corresponding weight (see Figure 2). A loop with no blob gets the usual weight of x, while a loop with a blob gets a modified weight y. Note that several blobs on the *same* loop reduce to a single blob. Obviously, only loops touching the left border can be blobbed.

This algebra has given rise to much work in recent years in the mathematical literature [8]. It has also been studied in the context of boundary conformal field theory [11] with results that have some small overlap with ours. (In [11] this algebra is called the "one boundary TL algebra", a name we shall not adopt.) The blob algebra is in fact a quotient of the more general affine Hecke algebra (like TL itself is a quotient of the ordinary Hecke algebra).

The representation theory of the two parameter algebra is richer than the representation theory of the TL algebra. For a given $x = q + q^{-1}$, and assuming first that $q = e^{i\gamma}$ is not a root of unity, exceptional cases occur whenever

$$y = \frac{\sin(r \pm 1)\gamma}{\sin r\gamma}, \quad r \text{ integer} \tag{2.3}$$

[In the original paper [7] this corresponds to $\eta = \mp r\gamma \mod \pi$ in the basic equation $y = \left(q - q^{-1}e^{2i\eta}\right) / \left(1 - e^{2i\eta}\right)$.]

In the case

$$y = \frac{\sin(r + 1)\gamma}{\sin r\gamma}, \quad r \text{ integer} \tag{2.4}$$

the spectrum of the hamiltonian

$$H = \frac{\gamma}{\pi \sin\gamma} \left(-ab - \sum_{i=1}^{N-1} e_i \right) \tag{2.5}$$

(the normalization guarantees unit sound velocity) has been studied in the continuum most recently in [11] where it was found **for any** $a > 0$ to give rise to the generating function of scaled gaps, in the

Figure 3: Vertices of the boundary loop model on the tilted square lattice. Bulk vertices are in any of two different states (corresponding to the generators 1 and e_i). Left boundary vertices are always blobbed (generator b), and right boundary vertices are unblobbed (generator 1).

sector with L non contractible lines[1] propagating:

$$K_{r,r+L} = \mathrm{Tr}\, q^{L_0 - c/24} = \frac{q^{h_{r,r+L}} - q^{h_{r,-r-L}}}{q^{c/24} P(q)} \tag{2.6}$$

Here, as usual, L_0 is a Virasoro generator,

$$c = 1 - \frac{6}{p(p+1)} \tag{2.7}$$

is the central charge for $\gamma = \frac{\pi}{p+1}$, and

$$h_{r,s} = \frac{[(p+1)r - ps]^2 - 1}{4p(p+1)} \tag{2.8}$$

are the conformal weights of the Kac table. Moreover, $P(q) = \prod_{n=1}^{\infty}(1-q^n)$. We stress that in (2.6) we have $q = \exp(2\pi i \tau)$, where τ is the standard modular parameter. As this meaning of q will be reserved for the argument of the spectrum generating functions, no confusion should arise with the *other* meaning of q as the quantum group deformation parameter $q = e^{i\gamma}$ appearing in the parameterization of x.

The case $r = 1$ of (2.6) is the usual hamiltonian for the loop model with free boundary conditions, since in this case $y = 2\cos\gamma = x$. In this case, the generating function of scaled gaps has indeed been known for a very long time [12] to be given by $K_{1,1+L}$. The case $n > 1$ as presented in [11] appeared to be new, although it is in fact related to results in [12] (and has algebraic connotations in terms of representation theory of the blob versus the Virasoro algebra). In this paper, we shall discuss (2.6) further, interpret it in the language of the loop model, and correct it whenever necessary.

We stress that the independence upon a is a truly remarkable phenomenon: it can be interpreted by saying that once the algebraic structure of the hamiltonian is decided, the continuum limit does not depend on the (boundary) details. Another way to view this independence is the following. The R matrix of the loop model with spectral parameter u, acting on strands i and $i+1$, can be written $R_i(u) = 1 + f(u)e_i$, and $f(u) = \frac{\sin(u)}{\sin(\gamma - u)}$ is easily found by solving the Yang-Baxter equations. Writing similarly the boundary matrix as $B(u) = 1 + g(u)b$, the Sklyanin (or reflection) equations relate $B(u)$ and $R_1(u)$, giving rise to a solution for $g(u)$ (see Eq. (40) in [13]) that contains an arbitrary constant of separation ζ. The arbitrariness of ζ is analogous to the a-independence discussed above.

3 Boundary loop model

We now want to study the blob algebra in the context of isotropic dense loop models, which are described by a transfer matrix instead of a hamiltonian. We recall that in the bulk, these models are defined by dense coverings of the (tilted) square lattice with self avoiding and mutually avoiding loops, each vertex allowing two possible configurations (see Figure 3 and also Figures 14–15 below), and each loop coming with a fugacity x. What happens at the boundary is the subject of this paper.

[1] A non contractible line is a strand propagating throughout the system. Thus, e_i acting on two non contractible lines at i and $i+1$ is zero by definition. Figure 2 has $L = 1$ non contractible line running from the bottom to the top of the figure (top and bottom are later wrapped onto an annulus). Note also that L and N must have the same parity.

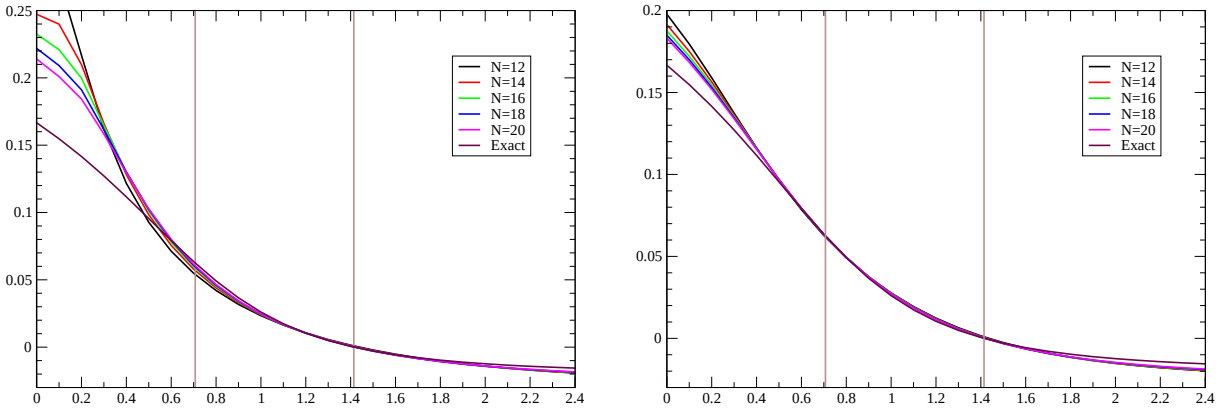

Figure 4: (Color online). Numerical check of the conjecture $h(y) = h_{r,r}$ as a function of y, here for $L = 0$ and $p = 3$ (the Ising model). The results were obtained from the finite-N corrections to the leading eigenvalue of the transfer matrix (3.2), obtained by exact diagonalization techniques, for widths up to $N = 20$. The left (resp. right) panel shows the choice $\lambda = 1$ (resp. $\lambda = \infty$), but the extrapolated results ($N \to \infty$) appear to be independent of λ. The vertical lines represent the particular values (2.4).

The sum over TL generators in the hamiltonian is replaced in that case by a product

$$T_0 = \prod_{i=1}^{\lfloor (N-1)/2 \rfloor} (1 + e_{2i}) \prod_{i=1}^{\lfloor N/2 \rfloor} (1 + e_{2i-1}) \tag{3.1}$$

where $\lfloor \ldots \rfloor$ denotes the integer part. By analogy we will supplement this by boundary contributions so the full transfer matrix reads

$$T = (1 + \lambda b) T_0 \tag{3.2}$$

In view of the a-independence of (2.6), we would expect the critical exponents associated with T to be independent of λ. This independence is checked numerically below (see Figure 4). From a geometrical point of view the most natural choice is then $\lambda = \infty$, so that after a trivial rescaling $T = bT_0$. This can be interpreted as a lattice model for which *every loop* touching the boundary gets a modified weight y instead of x. We will now study the conformal properties of this model (which we call the *boundary loop model*), as a function of x and y.

3.1 Conformal boundary conditions and critical exponents

The results from [12] and more recently [11] suggest the following. Recall the parametrization $x = 2\cos\gamma$; for each $y(r)$ we solve (2.4) to get r. This gives a *real* number $r \in (0, \frac{\pi}{\gamma})$. The leading eigenvalue in the loop model transfer matrix with L non contractible lines should scale with conformal weight $h(y) \equiv h_{r,r+L}$. For when $\gamma = \frac{\pi}{p+1}$ with p integer and $r = 1, 2, \ldots, p$ integer this is a rigorous consequence of [12] and the loop-RSOS correspondence, as will be discussed in Section 4 below.

Figure 4 serves the double purpose of checking this conjecture for $L = 0$ and $p = 3$ (the Ising model), and establishing the independence of the exponents on the choice of λ in (3.2). The agreement with the numerics is generally very good, and even in regions with strong corrections to scaling (in particular $y = 0$) it should be noted that the finite-N effects have consistently a trend and an amplitude compatible with the conjectured result in the thermodynamic limit. The choice $\lambda = \infty$ appears to

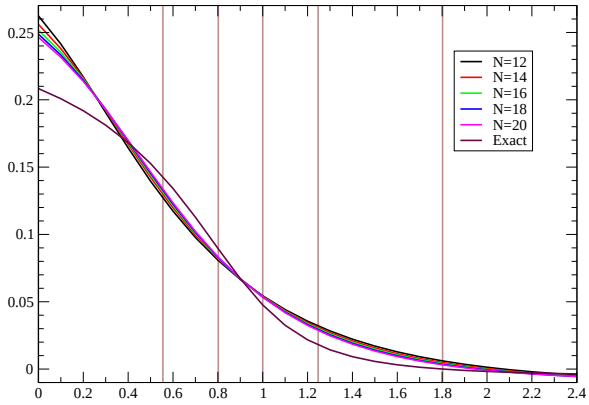

Figure 5: (Color online). Another check of the conjecture $h(y) = h_{r,r}$ for $L = 0$, here for $p = 6$ (the tricritical Potts model).

minimize the amplitude of the finite-size effects, and accordingly we shall invariably adopt this choice for the subsequent numerical checks.

Another check, still for $L = 0$ but with a higher value $p = 6$ (the tricritical Potts model), is shown in Figure 5.

From the point of view of the blob algebra, the parametrization (2.4) has nothing special compared with the other choice of sign in (2.3), which we rewrite here as

$$y(r') = \frac{\sin(r'-1)\gamma}{\sin r'\gamma} \tag{3.3}$$

Of course by using symmetries of the sine function we can write as well

$$y(r') = \frac{\sin(p+2-r')\gamma}{\sin(p+1-r')\gamma} \tag{3.4}$$

so we see that the associated exponent reads as well $h_{p+1-r',p+1-r'+L} = h_{r'-1,r'-L}$, by the symmetry of (2.8).

We now have to make things a little more precise and technical. The sector with L non contractible loops can in fact be considered from two points of view, depending on whether or not the leftmost non contractible loop is allowed to touch the left boundary. In Appendix A we discuss in details the sector structure of the transfer matrix bT_0 of (3.1) and show in particular that each of its eigenvalues corresponds to a definite choice: either the leftmost contractible loop is *forced* to touch the left boundary at least once, or it is *forbidden* from ever doing it. We shall henceforth refer to these two cases as the *blobbed* (resp. the *unblobbed*) sector. Note that in both sectors the contractible loops to the left of the leftmost non contractible loop may of course still touch the left boundary.

We claim that these two cases both correspond to conformal boundary conditions, which are different. For entropic reasons, the largest eigenvalue in the blobbed sector is obviously greater than the largest eigenvalue in the unblobbed sector. From the above arguments, the blobbed sector therefore has the exponent $h_{r,r+L}$ indeed. The unblobbed sector meanwhile has a different exponent $h_{r,r-L}$. This can be checked numerically, and is illustrated in Figure 6. Note of course that when $L = 0$ the two results actually coincide, as they should, since the two sectors are then identical.

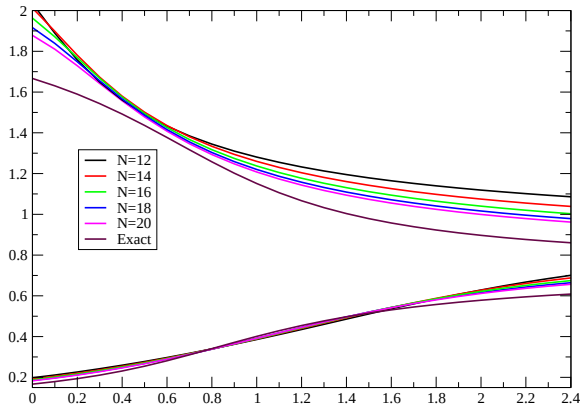

Figure 6: (Color online). Exponents $h(y)$ in the presence of $L = 2$ non contractible loops, here for $p = 3$ (the Ising model). The lower (resp. upper) curves show the numerical results for the (constrained) boundary loop model. They agree with the conjecture $h(y) = h_{r,r+L}$ (resp. $h(y) = h_{r,r-L}$) as claimed.

3.2 Relation to the Potts model

The boundary loop model is closely related to the $Q = x^2$ state Potts model at coupling (inverse temperature) J. Indeed, ignoring first boundary effects, the Potts model partition function can be written as [9]

$$Z = \sum_{\text{clusters}} \left(e^J - 1\right)^B Q^C = Q^{V/2} \sum_{\text{loops}} Q^{\ell/2} \tag{3.5}$$

The first sum is over bond percolation clusters consisting of B bonds and C connected components. The second sum is over loops on the medial lattice that separate the clusters and their duals, with ℓ being the number of loops and V the number of Potts spins. We have here supposed that the model is defined on a square lattice and stands at its critical temperature, $e^J - 1 = Q^{1/2}$. The equivalence between the cluster and loop formulations is obtained by applying the Euler relation. Note that the local configurations of the loops correspond precisely to the first two vertices of Fig. 3.

In the sector $L = 0$ we have claimed that the exponent of the boundary loop model is $h_{r,r}$ in the parameterization (2.4). We now wish to check that this claim is consistent with known results on the Potts model. To that end, consider the Q-state Potts model in the same annular geometry as the boundary loop model. Denote by P_1 and P_2 two points on the left boundary, and let boundary spins on the interval P_1P_2 be constrained to take a subset of $Q_{\rm s}$ states (with $Q_{\rm s} \leq Q$). In particular, when $Q_{\rm s} = 1$, this boundary condition corresponds to the Potts spins being fixed on the interval P_1P_2 and free on the remainder of the boundary. The modified partition function reads

$$Z(P_1P_2) = \sum_{\text{clusters}} \left(e^J - 1\right)^B Q^C \left(\frac{Q_{\rm s}}{Q}\right)^{C(P_1P_2)} = Q^{V/2} \sum_{\text{loops}} Q^{\ell/2} \left(\frac{Q_{\rm s}}{Q}\right)^{\ell(P_1P_2)} \tag{3.6}$$

where we have used the Euler relation as before. The number of clusters (resp. loops) that touch P_1P_2 is denoted $C(P_1P_2)$ (resp. $\ell(P_1P_2)$), and obviously we have $C(P_1P_2) = \ell(P_1P_2)$. We stress that C and ℓ still denote the *total* number of clusters and loops. Now, (3.6) is a special case of the boundary loop model with the correspondence between weights

$$\begin{aligned} Q &= x^2 \\ Q_{\rm s} &= xy \end{aligned} \tag{3.7}$$

In particular, for $Q_{\rm s}=1$ we have $r=p-1$ in (2.4). The corresponding special case of our general claim is therefore that the operator that changes the Potts model boundary conditions from free to fixed is $\phi_{p-1,p-1}=\phi_{1,2}$. This indeed coincides with a well-known result of Cardy [10].

Another verification is furnished by $Q=3$, $Q_{\rm s}=2$. The claim is then that the operator that changes the boundary conditions from free to mixed is $\phi_{2,2}$ with conformal weight $h_{2,2}=\frac{1}{40}$. This is again a well-known result.

3.3 Spectrum generating functions

Further numerical study shows that the spectrum generating functions for the blobbed and unblobbed sectors of the boundary loop model are simply the characters of generic irreducible representations of the Virasoro algebra, i.e., respectively,

$$\begin{aligned} \text{Blobbed sector:} \quad & Z_L^*(r)=\frac{q^{h_{r,r+L}-c/24}}{P(q)} \\ \text{Unblobbed sector:} \quad & Z_L(r)=\frac{q^{h_{r,r-L}-c/24}}{P(q)} \end{aligned} \tag{3.8}$$

This can be related with the structure of the basis of the blob algebra and the absence of truncation of the Bratelli diagram [7]. The precise finite-size definition of Z_L^* and Z_L in terms of the transfer matrix blocks T_L^* and T_L (defined in Appendix A). is given in (B.1)–(B.2); note that we have set $j=L/2$ in Appendix B.

The leading behavior in these expressions defines the exponents $h_{r,r\pm L}$ and has already been checked in Figs. 4–6 above. The coefficients of the terms up to level 6 in the development

$$1/P(q)=1+q+2q^2+3q^3+5q^4+7q^5+11q^6+\ldots \tag{3.9}$$

have been verified by computing the first 32 eigenvalues of T, for sizes up to $N=24$, and looking for integer gaps in the spectrum of critical exponents. For definiteness we have concentrated on the case $p=3$ and $L=2$. Independent computations were made in the blobbed and the unblobbed sectors. Moreover, the verification was made both for $y=x$ and for a generic value of y, and in either case the absence of singular vectors up to and including level 6 was ascertained.

It is important to stress that the spectrum generating functions are not given by (2.6) for the BLM. The full loop transfer matrix actually contains more information, but can be truncated when r is integer.

3.4 Partition function identities

We are now interested in the situation where the non contractible loops wrap around the annulus. The question then arises of which weight should be given to these loops (while our results for the exponents have some overlap with [11], the following has never appeared before). We will give in general the weight l to non contractible loops that do not touch the boundary (i.e., the outer rim of the annulus), and weight m to those that do (there is at most one). We now claim that the full partition functions are given by adding sectors $Z_L^*(r)$ and $Z_L(r)$ with the following amplitudes. We parametrize l, m in terms of two numbers α, β:

$$\begin{aligned} l &= 2\cosh\alpha \\ m &= \frac{\sinh(\alpha+\beta)}{\sinh\beta} \end{aligned} \tag{3.10}$$

Then the amplitudes are

$$\begin{aligned} D_L^* &= \frac{\sinh(L\alpha+\beta)}{\sinh\beta} \\ D_L &= \frac{\sinh(L\alpha-\beta)}{\sinh(-\beta)} \end{aligned} \tag{3.11}$$

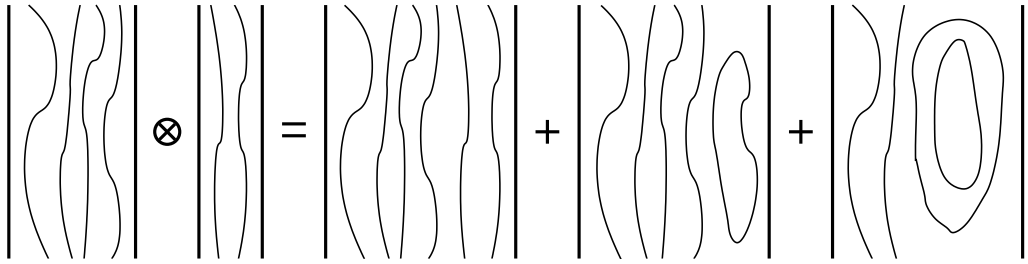

Figure 7: Pictorial representation of the recursion relation (3.13).

A complete proof of this statement is presented in Appendix B. Alternatively, we can argue that, because one can get from a sector L to a sector $L+2$ by adding two non contractible loops at the right of the annulus (here seen as a periodic strip), which can or not get contracted with the first L ones, the generic amplitudes have to obey a recursion relation (which has a deep algebraic nature, see [14]). Considering first the amplitudes D_L^0 for the simpler problem with transfer matrix T_0 (i.e., without the boundary generator b) one has

$$D_L^0 D_2^0 = D_L^0 + D_{L+2}^0 + D_{L-2}^0 \tag{3.12}$$

with initial values $D_0^0 = 1$ and $D_2^0 = l^2 - 1$. A pictorial rendering of this relation is shown in Figure 7. The solution reads explicitly $D_L^0 = U_L(l/2)$, where U_L is the Lth Chebyshev polynomial of the second kind. Turning now to the boundary loop model we must have similarly

$$\begin{aligned} D_L D_2^0 &= D_L + D_{L+2} + D_{L-2} \\ D_L^* D_2^0 &= D_L^* + D_{L+2}^* + D_{L-2}^* \end{aligned} \tag{3.13}$$

The initial values can then be determined to be $D_0 = D_0^* = 1$, $D_2 = l^2 - lm - 1$ and $D_2^* = lm - 1$, from which the general formulas (3.11) follow. In addition to the actual proof of Appendix B, we have checked (3.11) by formal manipulations of transfer matrices up to size $N = 6$, along the lines of [15].

The amplitudes can then be used to write down the general partition functions in the case N even (we set $L = 2j$)

$$Z = q^{-c/24} \left[\sum_{j=0}^{\infty} \frac{\sinh(2j\alpha + \beta)}{\sinh \beta} \, \frac{q^{h_{r,r+2j}}}{P(q)} - \sum_{j=1}^{\infty} \frac{\sinh(2j\alpha - \beta)}{\sinh \beta} \, \frac{q^{h_{r,r-2j}}}{P(q)} \right] \tag{3.14}$$

This partition function correspond to the most general case represented in Figure 8: contractible loops in the bulk get the weight x, those touching the boundary a weight y, non contractible loops not touching the boundary a weight l and the others a weight m.

The simplest situation occurs when

$$m = \frac{\sinh(r+1)\alpha}{\sinh r\alpha}\,, \tag{3.15}$$

that is, the parameter m has the same formal algebraic relationship with l that y does with x. Then $\beta = r\alpha$—the same r as in (2.4)—and one can write

$$Z = q^{-c/24} \left[\sum_{j=0}^{\infty} \frac{\sinh(2j + r)\alpha}{\sinh r\alpha} \, \frac{q^{h_{r,r+2j}}}{P(q)} - \sum_{j=1}^{\infty} \frac{\sinh(2j - r)\alpha}{\sinh r\alpha} \, \frac{q^{h_{r,r-2j}}}{P(q)} \right] \tag{3.16}$$

If moreover one is in a degenerate case where r is integer, one can reorganize the sum (3.16) into

$$Z = \sum_{j=0}^{\infty} \frac{\sinh(2j + r)\alpha}{\sinh r\alpha} \, K_{r,r+2j} - q^{-c/24} \sum_{j=1}^{r-1} \frac{\sinh(2j - r)\alpha}{\sinh r\alpha} \, \frac{q^{h_{r,r-2j}}}{P(q)} \tag{3.17}$$

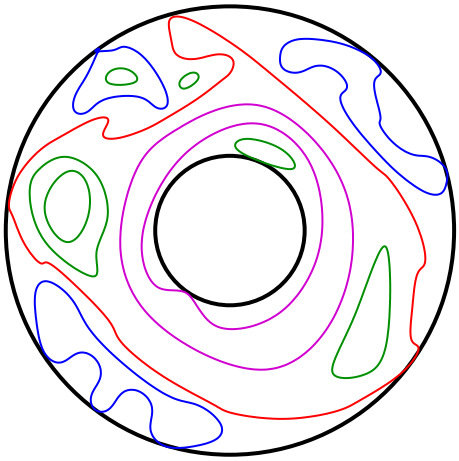

Figure 8: (Color online). The most general model studied in this paper. We distinguish four types of self-avoiding loops on the annulus: contractible loops touching (blue color in the figure) or not touching (green) the outer rim of the annulus, and similarly for non contractible loops (red or purple).

By pairing up terms with j and $r-j$ in the second sum, this can in turn be rewritten as

$$Z = \sum_{j=-[r/2]}^{\infty} \frac{\sinh(2j+r)\alpha}{\sinh r\alpha} K_{r,r+2j} \tag{3.18}$$

where $\lfloor \dots \rfloor$ denotes the integer part. When r is even, the contribution from $j = -r/2$ actually disappears. We thus get a sum over irreducible representations of the Virasoro algebra.

We claim that the subtractions occurring in the partition function do occur in finite size as well. These subtractions involve the conformal weights $h_{r,r+2j}$ and $h_{r,-r-2j}$ and correspond respectively to the blobbed sector with $L = 2j$ non contractible loops and the unblobbed sector with $L = 2j + 2r$. In other words, we claim there are level coincidences in finite size between the blobbed and unblobbed sectors when r is an integer: this in fact follows from the theory of representations of the blob algebra.

To be more precise, one can make sense of expressions such as (3.18) in finite size by replacing the definition (2.6) of the characters $K_{r,s}$ by traces of transfer matrix blocks, as outlined in Appendix B. Care should then be taken that the annulus is wide enough to accommodate the prescribed number of non contractible lines, which amounts to replacing the upper limit in the summation (3.18) by $N/2$. A numerical check of the level coincidences is shown in Table 1, for the case $N = 6$, $p = 6$ and $r = 1$ (i.e., $y = x$). We find indeed that the level spectrum of the transfer matrix (see Appendix A) block T_{2j+2r} is a *proper subset* of that of T^*_{2j}, for all allowed values of j (i.e., $j = 0, 1, \dots, N/2 - 2r - 1$). We have checked this statement for several other values of N, p and r, including on examples involving many more levels.

Although we have restricted to N even, similar results can be written for N odd, with the difference that L is odd (and thus never vanishes). The generating function then reads

$$Z = q^{-c/24} \left[\sum_{j=0}^{\infty} \frac{\sinh[(2j+1)\alpha+\beta]}{\sinh\beta} \frac{q^{h_{r,r+2j+1}}}{P(q)} - \sum_{j=0}^{\infty} \frac{\sinh[(2j+1)\alpha-\beta]}{\sinh\beta} \frac{q^{h_{r,r-2j-1}}}{P(q)} \right] \tag{3.19}$$

3.5 Neumann boundary conditions

If we go back to the derivation of the partition function for the $O(n)$ model [16] we see that Dirichlet boundary conditions for the $O(n)$ variable will translate into having a loop extremity on every point of the boundary, and the open lines thus obtained get a weight one (since the $O(n)$ variable is fixed to say $\vec{S} = (1, 0, \dots 0)$ on the boundary.) Let us assume this carries over to the fully packed case and our

f	T_0^*	T_2^*	T_4^*	T_6^*	T_2	T_4
-0.338946565198	1					
-0.295466694605		1				
-0.247750936031	1				1	
-0.238365774752		1				
-0.210311165453	1					
-0.201367085486		1				
-0.195052854163	1				1	
-0.184121456296		1				
-0.171718537721	1					
-0.168641596700			1			
-0.149149353298		1				
-0.134931152674			1			
-0.125859871619	1				1	
-0.110023422061	1					
-0.097996769822		1				
-0.085859268861		1	1			1
-0.069318933352	1				1	
-0.067354247176		1				
-0.048891555720	1				1	
-0.041781216253		1				
-0.036787385047			1			
-0.027592998174	1					
-0.012286435222		1				
-0.003076941021			1			
-0.000000000000				1		

Table 1: Complete set of levels for the various transfer matrix blocks (cf. Appendix A) in the case of $N = 6$ strands, for $p = 6$ (the tricritical Potts model) and $r = 1$ (i.e., $y = x$). The left column shows $-N^{-1} \log \lambda$ (rounded to 12 digits), where $\lambda \geq 1$ is the transfer matrix eigenvalue, and the remaining columns show the multiplicities of λ within the various blocks. A blank entry denotes zero multiplicity. The level coincidences mentioned in the text are clearly observed. (There is one extra coincidence of the level -0.085859268861, between T_2^* and T_4^*.)

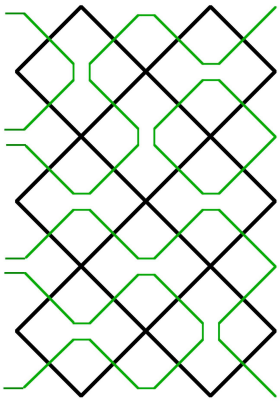

Figure 9: (Color online). Configuration in which the two boundaries of the annulus (here shown as a periodic strip) have respectively Dirichlet and Neumann boundary conditions. RSOS faces are shown in black, and the loops that separate clusters at constant height are green. The open lines going from the left to the left boundary carry unit weight.

geometry (see Figure 9) , where we thus demand that every point on the boundary looks like the top diagram on Figure 10, which we call a fork. We also require that open loops thus formed all carry a weight unity. It is then easy to see that this is equivalent to marking loops touching the boundary with a blob having parameter $y = 1$. In turn, with the usual parametrization for x we get the associated conformal weight to be

$$h_{\text{Twist}} = h_{p/2,p/2} = \frac{p^2-4}{16p(p+1)} \tag{3.20}$$

since $y = 1$ in (2.4) when $r = p/2$. This corresponds to a twist operator, or the dimension of the boundary field changing boundary conditions from Neumann to Dirichlet.

We note that this dimension of the twist operator agrees with the one proposed in [17] after some reinterpretation of the results. The formula given in this reference is slightly different

$$h^{\text{K}}_{\text{Twist}} = h_{\frac{p+1}{2},\frac{p+1}{2}} = \frac{(p+1)^2-4}{16p(p+1)} \tag{3.21}$$

but turns out to hold for the dilute phase of the $O(n)$ model [16] only [18]. For the dense case, it has to be replaced by (3.20).

We can now write the partition function with Dirichlet boundary conditions on one rim of the annulus and Neumann on the other, simply by setting $r = \frac{p}{2}$ in our formulas. An interesting limit to consider is then $p \to \infty$, $m = 1, l = 2$ where we find from (3.14)

$$Z = q^{-1/24} \sum_{j=-\infty}^{\infty} \frac{q^{(2j+1)^2/16}}{P(q)} \tag{3.22}$$

which is the usual Dirichlet-Neumann partition function for the free boson. The presence of the two kinds of terms $h_{r,r\pm L}$ in (3.14) is crucial to recover this limit.

Note that in the limit $p \to \infty$, the exponent $h(y)$ becomes a step function:

$$h(y) = \begin{cases} \frac{(L-1)^2}{4} & \text{for } y < 1 \\ \frac{(2L-1)^2}{16} & \text{for } y = 1 \\ \frac{L^2}{4} & \text{for } y > 1 \end{cases} \tag{3.23}$$

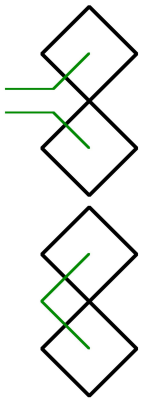

Figure 10: (Color online.) Two possible interactions between the loops and the left boundary: fork (top image) and blob (bottom image).

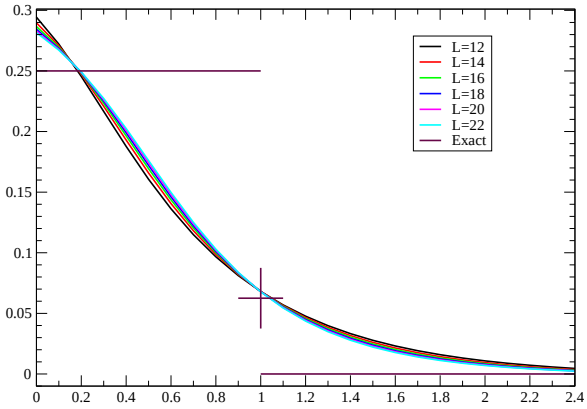

Figure 11: (Color online). Exponents $h(y)$ with $L = 0$ non contractible loops, in the limit $p \to \infty$. The exact result is a step function, passing through the value $h(1) = \frac{1}{16}$ (shown as a big cross).

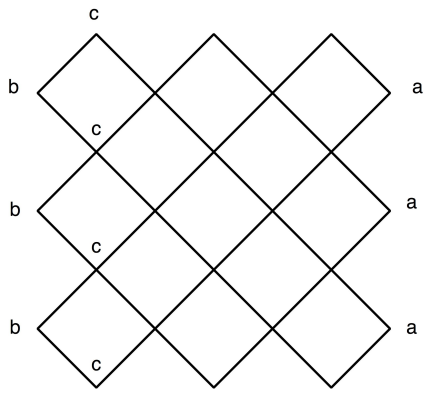

Figure 12: RSOS model in an annular geometry, for $N = 6$. Heights on the rightmost and the *two* leftmost layers are fixed as shown. Time flows vertically, and there are periodic boundary conditions in the time direction.

The numerical check, shown in Figure 11, is compatible with this behavior, although the finite-size corrections are of course large near the step.

Note that in general blob and fork do not coincide: this is true only when the associated weights are equal to unity. One can play the game of defining a fork algebra such that the top diagram in Figure 10 defines the fork operator f. Required relations to give to every open loop a weight z are then obviously

$$\begin{aligned} f^2 &= zf \\ e_1 f e_1 &= z e_1 \end{aligned} \tag{3.24}$$

But, by a rescaling $f \to f/z$ we get the same relations as the blob relations with $y = 1$!

4 Relation to RSOS models

We now want to tackle the boundary loop model by another route. Recall that in the numerical studies of Saleur and Bauer [12] it was found that for A_p RSOS models [with central charge (2.7)] the annulus partition function is exactly the character χ_{da} when the following boundary conditions are imposed: all heights on the right boundary of the annulus are fixed to a (Dirichlet boundary conditions) while on the left boundary, the heights on the boundary are fixed to b and those in the layer *next to the boundary* are fixed to c, with $d = \min(b, c)$.[2] Note that without the constraint on the next-to-leftmost heights, *each height* in that layer may take either of the values $b + 1$ and $b - 1$. This is illustrated in Figure 12.

Let us now see how this choice of boundary conditions translates in the loop model. To do so, we first note that if the loop model is defined on N strands, a time slice of the RSOS model is defined by $N + 1$ heights. A state of the model is a collection of those heights, denoted $|l_1, l_2, \ldots, l_{N+1}\rangle$, and we have the RSOS constraint $l_i = 1, 2, \ldots, p$ with $|l_{i+1} - l_i| = 1$. Figure 12 corresponds to a case of even N. We will restrict to this case to start. We will also restrict to the case where $c = b + 1$ so $b = d$, $c = d + 1$; note that then $d - a$ and N have the same parity.

We next recall briefly how the Temperley Lieb generators act in the RSOS representation. Taking

[2] In order to respect the use of a, b and c in Ref. [12], note that throughout Section 4, a is not the parameter of (2.5), b is not the blob generator in (2.2), and c is not the central charge (2.7).

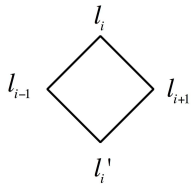

Figure 13: Labelling of RSOS heights around a lattice face.

the time to flow downwards in Figure 13, the generator e_i acts as

$$e_i\ |l_1,\ldots,l_{i-1},l_i,l_{i+1},\ldots,l_{N+1}\rangle = \delta(l_{i-1},l_{i+1})\sum_{l_i'}\frac{(S_{l_i}S_{l_i'})^{1/2}}{S_{l_{i-1}}}\ |l_1,\ldots,l_{i-1},l_i',l_{i+1},\ldots,l_{N+1}\rangle \quad (4.1)$$

where the S_l are the components of the Perron-Frobenius eigenvector of the adjacency matrix of A_p, and read explicitly

$$S_l = [l]_q = \frac{\sin\left(\frac{l\pi}{p+1}\right)}{\sin\left(\frac{\pi}{p+1}\right)} \quad (4.2)$$

where we have introduced the q-deformed numbers $[l]_q \equiv (q^l - q^{-l})/(q - q^{-1})$.

The transfer matrix of the RSOS model has the usual form (3.1), but now in terms of the e_i defined by (4.1). The graphical expansion of the partition function is obtained by taking, for each elementary face transfer matrix $1 + e_i$, either the identity—in which case a vertical bar is drawn diagonally across the face, indicating that $l_i = l_i'$ for this term—or the Temperley Lieb generator e_j, in which case a horizontal bar is drawn, indicating that $l_{i-1} = l_{i+1}$. One gets in this way clusters of constant heights, which can be separated by non intersecting loops drawn on the dual lattice.

The analysis of the weights needs some modification as compared to Pasquier's original treatment [19] of the RSOS model on a torus, but some of the key elements can be taken over. We first consider the case of $l_1 = l_{2N+1} \equiv d$; the heights l_2 are also fixed and we shall assume $l_2 = d + 1$ (the case $l_2 = d - 1$ being similar). We further assume that there is at least one cluster connecting the left and right boundary of the annulus (in the limit where the aspect ratio $\rho = M/N \to \infty$ this is almost surely the case). There is then $L = 0$ non contractible lines. Since all clusters connecting the two boundaries have the same height d, we might just as well identify them. In the graphical expansion this can be represented by adding extra vertical bars on the two boundaries.

With this identification it follows that any loop is at the junction between exactly *two* distinct clusters. Now orient every loop in the clockwise direction. When traversing any loop along this direction, the cluster to its right is said to be surrounded by the loop, whereas the cluster to its left is said to surround the loop. Let us now represent each distinct cluster by a node, and each loop by a directed link going from the cluster that it surrounds towards the cluster that it is surrounded by. This then defines a directed rooted tree, where every link is oriented towards the root, the root being the *unique* cluster connecting the two boundaries.

The weight appearing in (4.1) is then distributed on individual loop turns as follows: Consider a loop that surrounds a cluster at height l and that is surrounded by a cluster at height k. When making a right (resp. left) turn whilst being tangential to a *horizontal* bar, the loop picks up a factor $(S_l/S_k)^{1/2}$ (resp. $(S_l/S_k)^{-1/2}$). Turns being tangential to a vertical bar do not carry any weight. The complete loop, being clockwise, makes four more right than left turns, but only two of those excess turns carry any weight, so the complete weight is S_l/S_k.

The directed tree is now undone by summing over the heights of its nodes. We start at a leave node. For any fixed height k of the node adjacent to the leaf, the height of the leaf node can be $l = k \pm 1$. Summing over l gives a weight[3] $(S_{k+1} + S_{k-1})/S_k = 2\cos\left(\frac{\pi}{p+1}\right)$—note that this is *independent* of

[3]This is true even when $l = 1$ or $l = p$, since $S_0 = S_{p+1} = 0$ from (4.2).

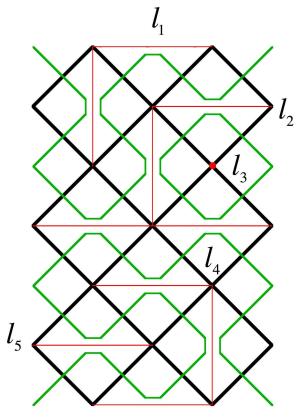

Figure 14: (Color online.) Configuration of the RSOS clusters (in red color) for a case where $a = d$. Periodic boundary conditions are imposed in the time (vertical) direction.

k—which can be attributed to the loop represented by the link directed away from the leaf. We then remove the leaf and its outgoing link, and proceed iteratively, moving always from the leaves and towards the root. A special case occurs when summing over the heights of those nodes adjacent to the root whose outgoing link corresponds to a loop that touches the left boundary. Indeed, the heights of those nodes have been fixed to $d+1$, and we obtain then the weight $S_{d+1}/S_d = [d+1]_q/[d]_q$. Finally, when the whole tree has been undone, only the root node remains, but since its height is fixed it contributes no additional weight.

Consider now the loop model with weights $x = 2\cos\left(\frac{\pi}{p+1}\right)$ and $y = [d+1]_q/[d]_q$—i.e., setting $r = d$ in (2.4)—and no non contractible lines, $L = 0$. Its configurations are in one-to-one correspondence with those of the RSOS model treated above and the weights x, y are the same. The spectrum of $T_{\rm loop}$ therefore contains the complete spectrum of $T_{\rm RSOS}$, and we have verified this numerically. In particular the leading eigenvalues of these transfer matrices coincide. However, $T_{\rm loop}$ also contains eigenvalues not present in $T_{\rm RSOS}$. This was to be expected, since the loop model contains non-local information not present in the RSOS model (allowing in particular its definition for non-integer p).

An example of the loop-RSOS equivalence is illustrated in Figure 14, still for the case $d = a$. Denoting by $l_1, \ldots, l_5$ the heights of the five clusters[4] (labelled from top to bottom) we find the overall weight (for simplicity we denote $[l]_q \equiv l$):

$$\frac{(l_2 l_5)^{1/2}}{l_1}\frac{(l_1 l_3)^{1/2}}{l_2}\frac{(l_1 l_4)^{1/2}}{l_2}\frac{(l_3 l_4)^{1/2}}{l_2}\frac{(l_2 l_5)^{1/2}}{l_4}\frac{l_4}{l_5} = \frac{l_3}{l_2}\frac{l_4}{l_2} \tag{4.3}$$

Note that $l_4 = l_1$ by the periodic boundary conditions in the time direction. Each of the two factors on the right-hand side is associated with a loop. Since l_3 can take values $d \pm 1$ while $l_2 = l_5 = d$ and $l_4 = l_1 = d+1$, the overall weight is $2\cos\left(\frac{\pi}{p+1}\right) \times \frac{S_{d+1}}{S_d} = xy$ as claimed.

While this construction clearly works when there are no non contractible lines running through the annulus (ie, $a = d$), things are more delicate when there are. Figure 15 shows for instance that a configuration with two non contractible lines does not necessarily contribute to $d = 3$, $a = 1$. A little thought suggests to simply eliminate non contractible loops touching the boundary in this case.

We have indeed checked numerically that when $d - a$ is negative, the eigenvalues of the RSOS model are all found in the loop transfer matrix for the blobbed sector, and the leading eigenvalues coincide. Meanwhile if $d - a$ is positive, this is true provided one considers instead the unblobbed sector for the loop model. In both cases one needs to have $L = d - a$ and $y = y(d)$.

[4] Note that in this example the subscripts are used differently than in (4.1).

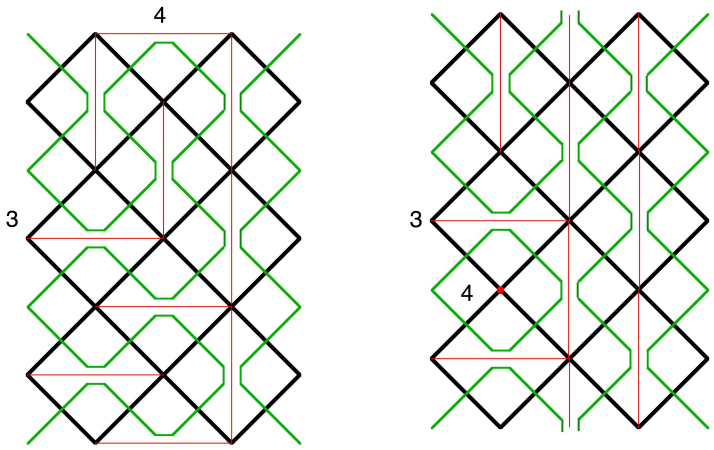

Figure 15: (Color online.) The choice $a = 3, b = 4, c = 1$ is not compatible with the configuration of loops shown on the left panel (even though there are two non contractible loops). It is however compatible with the configuration shown on the right panel.

This corresponds simply to accepting configurations such as the one on the right of Figure (15), but not the one on the left.

Of course the RSOS model contains more situations: one can decide to have $c = b - 1$ instead, or to have N odd. The complete set of rules is as follows:

$$\begin{array}{llll} d-a>0 \text{ and has same parity as } N: & L=|d-a|, & y=y(d), & \text{unblobbed} \\ d-a\leq 0 \text{ and has same parity as } N: & L=|d-a|, & y=y(d), & \text{blobbed} \\ d-a\geq -1 \text{ and has opposite parity of } N: & L=|d+1-a|, & y=y(p-d), & \text{blobbed} \\ d-a<-1 \text{ and has opposite parity of } N: & L=|d+1-a|, & y=y(p-d), & \text{unblobbed} \end{array} \tag{4.4}$$

The first two cases coincide with what we discussed if N is even and generalize it easily if N is odd. In these two cases, the left boundary necessarily sees $b = d + 1$, $c = d$, and the value of y follows from the analysis of the loop model.

The last two cases meanwhile require that $b = d$, $c = d + 1$. The new value of y giving the correct weights to the boundary loops is thus $y = [d]_q/[d + 1]_q$, which coincides with $y = [p + 1 - d]_q/[p - d]_q$.

Note that the rules (4.4) are compatible with the global symmetry $l_i \to p - l_i$ of the RSOS model configurations and weights (4.2). On the level of the sectors this reads $(d, a) \to (p - d, p + 1, a)$ and is nothing but the usual symmetry of the Kac table (2.8).

An extensive numerical check of (4.4) is given in Table 2. We show all levels observed for the RSOS model with $N = 6$ and $p = 6$, along with the sector label (d, a), and we give the corresponding multiplicities of these levels in the loop model, where each sector $T_L^{(*)}(r)$ is characterized by the number of non contractible lines L, the blobbing of the leftmost string ($*$ denotes the blobbed sector), as well as r which determines the boundary weight $y(r)$ through (2.4). Remarkably, *all of the RSOS levels are also observed in the loop model*, with the sector given precisely by the rules (4.4). This observation extends to other values of N and p (with any parities).

Note that the dimension of the loop (resp. RSOS) model transfer matrix does not (resp. does) depend on r. This apparent paradox is resolved by the fact that a given loop model sector contains in general extra eigenvalues (not shown in Table 2) which are not present in the RSOS model. It should also be noted that the dominant eigenvalue in a given RSOS sector is always observed to be dominant as well in the corresponding loop model sector (4.4).

Finally, we should mention a couple of fine details. In general the levels are not observed to be degenerate. One exception visible in Table 2 is that the level $f = -0.036787385047$ is present in two distinct sectors, but since this is so both on the RSOS and the loop side, definite labels respecting (4.4) can be assigned as shown in the table. Another exception is the level $f = -0.085859268861$ which

f	(d,a)	T_0^*					T_2^*				T_4^*		T_2			T_4	
	r	1	2	3	4	5	1	2	3	4	1	2	3	4	5	1	5
-0.338946565198	(1,1)	1															
-0.324025479536	(2,2)		1														
-0.316673567023	(3,3)			1													
-0.310464485251	(2,3)				1												
-0.302390277235	(1,2)					1											
-0.295466694605	(1,3)						1										
-0.291196112101	(2,4)							1									
-0.289510241627	(3,2)								1								
-0.288254559167	(2,1)									1							
-0.241054964628	(2,2)		1														
-0.238365774752	(1,3)						1										
-0.237748281915	(3,3)			1													
-0.234731074254	(2,3)				1												
-0.230275094022	(2,4)							1									
-0.230197803440	(1,2)					1											
-0.226587692821	(3,2)								1								
-0.223700268691	(2,1)									1							
-0.220405235066	(3,1)												1				
-0.212046452393	(2,5)													1			
-0.210311165453	(1,1)	1															
-0.201367085486	(1,3)						1										
-0.200352797500	(1,4)														1		
-0.194920765586	(2,2)		1														
-0.191048760878	(2,4)							1									
-0.187939781596	(2,2)		1														
-0.186511467791	(3,2)								1								
-0.186351229891	(3,3)			1													
-0.184916564626	(3,3)			1													
-0.184121456296	(1,3)						1										
-0.183007717844	(2,1)									1							
-0.182528404723	(2,3)				1												
-0.179523463630	(1,2)					1											
-0.178529556360	(2,3)				1												
-0.176928229253	(2,4)							1									
-0.172266060806	(3,2)								1								
-0.171718537721	(1,1)	1															
-0.170284900502	(3,1)												1				
-0.168641596700	(1,5)										1						
-0.167982529467	(2,6)											1					
-0.163038059540	(2,5)													1			
-0.155628452273	(2,2)		1														
-0.153242699723	(1,4)														1		
-0.149149353298	(1,3)						1										
-0.147179401602	(3,3)			1													
-0.140243221820	(2,4)							1									
-0.139719837688	(2,3)				1												
-0.135157811358	(3,2)								1								
-0.134931152674	(1,5)										1						
-0.132209035214	(2,6)											1					
-0.115345804299	(2,2)		1														

f	(d,a)	T_0^*					T_2^*				T_4^*		T_2			T_4	
	r	1	2	3	4	5	1	2	3	4	1	2	3	4	5	1	5
-0.110023422061	(1,1)	1															
-0.109559975348	(3,3)			1													
-0.105095398499	(3,1)												1				
-0.104419222242	(2,3)				1												
-0.099484992148	(2,5)													1			
-0.097996769822	(1,3)						1										
-0.097573977039	(1,2)					1											
-0.095502814093	(2,2)		1														
-0.092050608093	(1,4)														1		
-0.088269162793	(3,3)			1													
-0.086753609983	(2,4)							1									
-0.085859268861	(1,5)						1				1					1	
-0.085433490626	(2,4)							1									
-0.085246090691	(3,2)								1								
-0.085077485734	(2,1)									1							
-0.082112734265	(2,3)				1												
-0.080981552646	(3,2)								1								
-0.080291708506	(2,6)											1					
-0.067354247176	(1,3)						1										
-0.066058643675	(3,3)			1													
-0.064397781477	(2,3)				1												
-0.061125554776	(1,2)					1											
-0.059945596252	(2,4)							1									
-0.056741093622	(3,2)								1								
-0.054049770890	(2,1)									1							
-0.052888923290	(2,5)													1			
-0.044940510316	(1,4)														1		
-0.041781216253	(1,3)						1										
-0.037564796511	(2,2)		1														
-0.036787385047	(1,5)										1						
-0.036787385047	(1,6)																1
-0.033076470754	(2,4)							1									
-0.032439276523	(3,3)			1													
-0.030419378593	(2,6)											1					
-0.028358275153	(3,2)								1								
-0.027839432948	(2,3)				1												
-0.027592998174	(1,1)	1															
-0.020938336515	(3,1)												1				
-0.015656249492	(2,2)		1														
-0.012286435222	(1,3)						1										
-0.012266183325	(2,5)													1			
-0.007688713211	(3,3)			1													
-0.005272945987	(2,4)							1									
-0.003076941021	(1,5)										1						

Table 2: Complete set of levels for the various sectors (d,a) of the RSOS model, here for size $N = 6$ and $p = 6$ (the tricritical Potts model), cf. Table 1. The left column shows $-N^{-1}\log\lambda$ (rounded to 12 digits), where $\lambda \geq 1$ is the transfer matrix eigenvalue. The remaining columns show the corresponding multiplicities of λ within the various sectors $T_L^{(*)}$ of the loop model (the asterisk $*$ denotes the blobbed sector, see Appendix A). A blank entry denotes zero multiplicity. The boundary weight $y = y(r)$ is given by (2.4), with r indicated in the top of the table.

apart from its assignment to $T_4^*(r=1)$ by (4.4) appears also in two more loop sectors, $T_2^*(r=1)$ and $T_4(r=1)$. This type of degeneracies can be explained by quantum group arguments.

Recall now that the character of the irreducible representation of the Virasoro algebra with highest weight h_{da} can be written as [20]

$$\chi_{da} = \sum_{n=0}^{\infty} K_{d,a+2(p+1)n} - \sum_{n=1}^{\infty} K_{d,2n(p+1)-a} \tag{4.5}$$

We wish to recover this character from the knowledge of the loop model partition function. This involves as usual an infinite series of additions and subtractions of sectors which is made possible in finite size by the quantum group symmetry. We suppose we are in the situation with heights $b = d, c = d+1$. To go from d on the left side to a on the right side we need to sandwich between the left and the right the adjacency matrix of the A_p diagrams so that a random walk on this diagram, from boundary to boundary, hopping from non contractible cluster to non contractible cluster, takes one from b to a. All the steps are identical with those in [12] where partition functions with boundary conditions fixed at the leftmost and rightmost sides were computed. Using the eigenvectors of the adjacency matrix as in equation (4.15-4.19) of [12], the required expression is thus (we have set $H = p+1$)

$$\frac{2}{H} \sum_{p=1}^{H-1} \sin\left(\frac{\pi p d}{H}\right) \sin\left(\frac{\pi p a}{H}\right) Z\left(\alpha = \frac{i\pi p}{H}, \beta = d\alpha\right) \tag{4.6}$$

Here Z is calculated with α running over $\frac{i\pi p}{H}$ and for each α the value of m—the weight of non contractible loops—follows from the same argument as in the case of the leading exponent $r=1$ in the bulk case, implying $\beta = d\alpha$ so $m = \frac{\sinh(d+1)\alpha}{\sinh d\alpha}$, $\alpha = \frac{i\pi p}{H}$. Using the expression (3.18) we see that the functions $K_{d,d+2j}$ $(r=d)$ get a combinatorial factor

$$\frac{2}{H} \sum_{p=1}^{H-1} \frac{1}{2} \left[\cos(2j+d-a)\frac{p\pi}{H} - \cos(2j+d+a)\frac{p\pi}{H}\right] \tag{4.7}$$

Since $d-a$ and $2j$ have the same parity, this select the conditions

$$\begin{aligned} 2j+d-a &= 2n_1 H \\ 2j+d+a &= 2n_2 H \end{aligned} \tag{4.8}$$

for the first and second term respectively. Remembering that j runs only from $-[r/2]$ to infinity, and that when the foregoing conditions are satisfied one gets a factor $\frac{H}{2}$ from the sum cancelling the prefactor in (4.6), it follows that

$$Z = \sum_{n=0}^{\infty} K_{d,a+2nH} - \sum_{n=1}^{\infty} K_{d,-a+2nH} \tag{4.9}$$

which is the result we wanted.

5 More algebraic considerations

There are many ways to think of the blob algebra. We would like now to think of it within the theory of cabling, i.e., tensor products of spin 1/2 representations of $U_q(sl_2)$. Consider therefore $r+1$ representations of spin 1/2, and suppose we wish to project them on the maximally q-symmetric representation. The object doing this is the q-symmetrizer, whose expression is well known by induction to be [21]

$$\mathcal{S}_{r+1}(e_1, \ldots, e_r) = \mathcal{S}_r - t_r \mathcal{S}_r e_r \mathcal{S}_r \tag{5.1}$$

with the boundary condition $\mathcal{S}_1 = 1$. Here the t_r are numbers given by

$$t_r = \frac{\sin r\gamma}{\sin(r+1)\gamma} \tag{5.2}$$

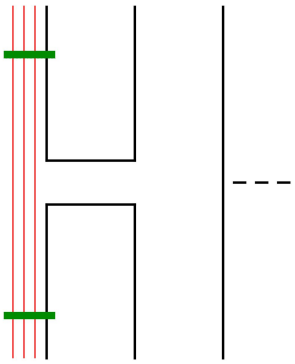

Figure 16: (Color online.) Ghost strings $2-r,\ldots,0$, represented by thin red lines. They are symmetrized among themselves and with the first real line (the symmetrization is shown symbolically by horizontal green bars).

and the e_i are TL generators which obey (2.1) as before and act on the tensor product of the i'th and $(i+1)$'th spin 1/2 representation. These generators will not be identified with the ones used in the previous sections however (see below). The first values are well known: $\mathcal{S}_1 = 1$, $\mathcal{S}_2 = 1 - \frac{e_1}{2\cos\gamma}$, etc.

Let us now add to our system $r-1$ "ghost strings" as in figure 16 (labelled $2-r,\ldots,0$) on which generators $e_{2-r},\ldots,e_0$ act, and let us symmetrize on these ghost strings and the first one of our system. We then define b_r through

$$b_r = \mathcal{S}_r(e_{2-r},\ldots,e_0) \tag{5.3}$$

We have then

$$\begin{aligned} b_1 &= 1 \\ b_2 &= 1 - \frac{e_0}{2\cos\gamma} \\ b_3 &= 1 - t_2(e_{-1}+e_0) + t_1 t_2(e_{-1}e_0 + e_0 e_{-1}) \end{aligned} \tag{5.4}$$

and so on. By construction, the b_r's are projectors

$$b_r^2 = b_r \tag{5.5}$$

It is easy to show that they satisfy moreover

$$e_1 b_r e_1 = \frac{\sin(r+1)\gamma}{\sin r\gamma} e_1 P_{r-1} \tag{5.6}$$

where we denote by P_{r-1} the symmetrizer on the ghost strings only, $P_{r-1} = \mathcal{S}_{r-1}(e_{2-r},\ldots,e_{-1})$. Of course, $[e_i, P_{r-1}] = 0$ for all $i \geq 1$. We can thus consider a modified version of the TL algebra where instead of the generators e_i we have the modified generators $\tilde{e}_i \equiv P_{r-1}e_i$. They obviously satisfy the bulk TL relations (2.1), since P_{r-1} is a projector. Moreover we now have the relations (2.2) of the blob algebra, with $b = b_r$ and (2.4). We have thus made the link with the foregoing discussion and shown that for r an integer, the boundary conditions corresponding to the value (2.4) can be obtained by adding ghost strings on the left boundary and symmetrizing them with the first "real string" in the system.

This should not come as a surprise: it is easy to show using Pasquier's 6j calculations [22] that the insertion of b_r through the ghost strings construction translates into RSOS language by having heights increasing linearly from the left hand side of the ghost strings up to the first height from $l = 1$ to

$l = r$, and then because b_r symmetrizes on r strings and thus on the first real string as well, from $l = r$ to $l = r + 1$. This proves that the transfer matrix bT_0 describes exactly the mixed RSOS boundary conditions.

Note that one does not have to introduce the ghost strings. Algebraically, the same would be obtained by replacing these $r-1$ strings by a spin $\frac{r-1}{2}$ (in which case, $P_{r-1} = 1$ identically). The operator b_r then amounts to projecting the product of this representation and the first spin $1/2$ representation onto spin $r/2$.

In this form, the identification was already mentioned in [12].

The formulas obtained in this section should match the ones which appeared in a recent paper by Pearce et al. [23]; the derivation there is based on boundary integrability, and does not refer to the blob or boundary Temperley Lieb algebra, as far as we can see.

6 Conclusion

In conclusion, it is important to stress that we have found a continuum of conformal boundary conditions for the dense loop models. How to incorporate them into a consistent conformal field theory remains an open problem. Note that none of these boundary conditions involves the *number of times loops touch the boundary*, which would correspond somehow to modified spin-spin couplings on the boundary. Rather, giving a different weight y to loops touching the boundary can be interpreted in the $O(n)$ model most easily as restricting the degrees of freedom on the boundary to take values in a sub manifold of 'dimension' y. This is not without reminding us of results in the WZW cases [24].

The results described in this paper point to many further directions. Among those are:
- geometric applications of the generating functions on the annulus
- derivation of the Bethe ansatz equations and of the spectrum of scaled gaps
- extensions to the dilute case
- extension to the double boundary case
- study of boundary conditions in $c = 1$ theories

We hope to report on these soon. To conclude, we now give one example of application. We consider the case $x = 0$, $c = -2$ and the partition function with $x = l = 0$, $y = m = 1$ (i.e,. loops touching the boundary get a weight one, whether contractible or not, the others are not allowed). After some simple manipulations, (3.14) can be written as

$$Z = \frac{q^{-1/24}}{P(q)} \sum_{j=-\infty}^{\infty} (-1)^j q^{(4j-1)^2/32} \tag{6.1}$$

This is easy to interpret geometrically as the partition function of a gas of dense loops, all contractible, which are all constrained to touch the left boundary. The loops can also be replaced by trees. Meanwhile, this partition function can also be interpreted in the symplectic fermion theory [25].

Acknowledgments: H. Saleur thanks I. Kostov and V. Schomerus for many interesting discussions, and for communication of their unpublished results [18, 25].

Note added in proof: After the completion of this work, I. Kostov has studied (in the preprint hep-th/0703221) the coupling of our boundary loop model to two-dimensional quantum gravity. His results corroborate those presented here.

A Transfer matrix structure

In this Appendix we discuss the construction and structure of the transfer matrix of the boundary loop model, corresponding to taking the limit $\lambda \to \infty$ in (3.2).

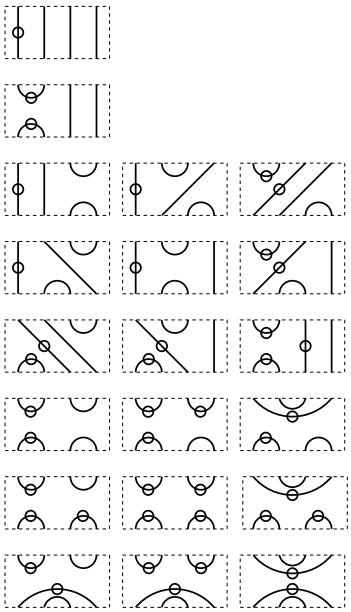

Figure 17: Ordering of the states of the transfer matrix T, here for width $N = 4$ strands.

We recall the most general case of the boundary loop model, cf. Fig. 8. The model is defined on an annulus with the exterior boundary being distinguished. Each loop touching at least once this boundary gets a weight y if it is contractible (i.e., homotopic to a point), and m if it is not. Each loop that never touches the distinguished boundary gets a weight x if it is contractible, and l if it is not. For an annulus of width N strands (we assume N even) and circumference M, this defines a partition function $Z_{N,M}(x, y, l, m)$ which can be expressed in terms of the M'th power of the transfer matrix $T = bT_0$, where T is given in terms of TL generators by (3.1), and the generators b, e_i obey the blob algebra $B_N(x, y)$ defined by (2.1)–(2.2).

For simplicity we henceforth represent the annulus as a rectangle of width N and height M, with periodic boundary conditions identifying its top and bottom sides. The distinguished boundary is taken to be the left side. The transfer matrix then acts on states which can be depicted graphically as fully-packed non-crossing link patterns within a slab bordered by two horizontal rows, each of N points. A link joining the top and the bottom row is called a *string*, and any other link is called an *arc*. The action of a word in $\mathcal{B}_N(x, y)$ on a state is obtained by adjoining the word to the top row of the slab (i.e., time propagates upwards). The 20 possible states for $N = 4$ are represented in Fig. 17.

Note that links touching a point on the left boundary are necessarily blobbed (shown by a circle in Fig. 17). Only links up to and including the leftmost string can be blobbed. The states can be ordered as follows: First we sort the states according to a decreasing number of strings L. For fixed $L > 0$, we place first the states in which the leftmost string is unblobbed. And finally we group together states with fixed L and fixed blobbing of the leftmost string, according to the link/arc configuration of the lower row of the slab. This gives the order of the rows of Fig. 17. The ordering of states within each row is according to the link/arc configuration of the upper row of the slab.

With this ordering of the states, T has a blockwise lower triagonal structure, with each block corresponding to a group of states as defined above. The reason is that acting by e_i can annihilate two strings (if their positions on the top side of the slab are i and $i + 1$) but cannot create any strings. Likewise, acting by b can blob the leftmost string, but it cannot subsequently be unblobbed. The triagonal structure implies that the eigenvalues of T are the union of eigenvalues of the blocks on its diagonal. Moreover, blocks differing only by the configuration of the bottom row are identical. For the purpose of studying only the spectrum of T the bottom row can therefore be completely forgotten, leading to a much smaller transfer matrix.

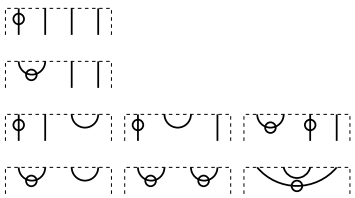

Figure 18: Reduced states for $N = 4$.

Indeed let us define a *reduced state* as a non-crossing link pattern on N points. A (full) state can be turned into a pair of reduced states by cutting each of its strings and pulling apart the upper and lower parts. For convenience, a cut string will still be called a string with respect to the reduced state. For $N = 4$ there are 8 reduced states, shown in Fig. 18.

The blocks on the diagonal of T are denoted T_L and T_L^*, where L is the number of strings, and the presence (resp. absence) of the asterisk $(*)$ indicates that the leftmost link is blobbed (resp. unblobbed). Note that the blocks T_L and T_L^* can be constructed in terms of the reduced states. The numerical studies of the spectral properties of T reported in this paper were done by diagonalizing these blocks in the basis of reduced states. Their dimensions read (see Appendix B for proofs of closely related statements)

$$\begin{aligned} \dim T_L &= \binom{N-1}{(N-L-2)/2} \quad \text{for } L = 0, 2, \ldots, N-2 \\ \dim T_L^* &= \binom{N-1}{(N-L)/2} \qquad \text{for } L = 2, 4, \ldots, N \end{aligned} \tag{A.1}$$

With the terminology being fixed, the annulus partition function can now be written as [15]

$$Z_{N,M}(x, y, l, m) = \langle u | T^M | v \rangle \ . \tag{A.2}$$

Here, the right vector $|v\rangle$ is the unit vector corresponding to the state with N strings. The left vector $\langle u|$ is obtained by identifying the top and bottom rows for each state; counting the number of loops of each type (contractible or not, blobbed or not) gives the corresponding weight as a monomial in x, y, l, and m. For instance, with $N = 4$ and the ordering of the states shown in Fig. 17, we have

$$\begin{aligned} |u\rangle &= (1, 0, 0, \ldots, 0) \\ |v\rangle &= (l^3 m, l^2 y, lmx, lm, y, \ldots, xy) \end{aligned} \tag{A.3}$$

B Exact eigenvalue amplitudes

The goal of this Appendix is to provide a rigorous combinatorial proof of the amplitude formulae (3.11) by generalizing the working of [26]. The discussion assumes knowledge of the transfer matrix blocks T_L and T_L^* defined in Appendix A.

Following [26], we introduce the *characters*

$$K_k = \mathrm{Tr}\,(T_{2k})^M, \qquad K_k^* = \mathrm{Tr}\,(T_{2k}^*)^M\,, \tag{B.1}$$

where we stress that the trace is over *reduced* states. Also, let Z_j (resp. Z_j^*) be the annulus partition function constrained to have exactly $2j$ unblobbed non contractible loops (resp. $2j-1$ unblobbed and 1 blobbed non contractible loops). In other words, Z_j (resp. Z_j^*) consists of the terms in the full partition function $Z_{N,M}(x, y, l, m)$ whose l, m dependence is l^{2j} (resp. $l^{2j-1}m$). The goal is to search

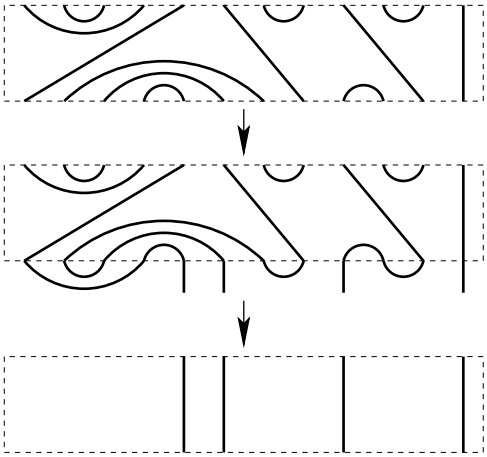

Figure 19: Construction of invariant restricted states. (a) A configuration contributing to Z_j with $N = 12$ and $j = 2$, here depicted as a state. (b) Application on the bottom of the reduced state corresponding to the top half of (a). (c) After removal of arcs one has simply $2j$ links.

for a decomposition of the form

$$\begin{aligned} Z_j &= \sum_{k=j}^{N/2} \left[D_k^{(j)} l^{2k} K_k + D_{k*}^{(j)} l^{2k-1} m K_k^* \right] \\ Z_j^* &= \sum_{k=j}^{N/2} \left[D_k^{(j)*} l^{2k} K_k + D_{k*}^{(j)*} l^{2k-1} m K_k^* \right] , \end{aligned} \tag{B.2}$$

where $D_k^{(j)}$, $D_{k*}^{(j)}$, $D_k^{(j)*}$, and $D_{k*}^{(j)*}$ are coefficients to be determined. In the notation of (3.11) we have then

$$\begin{aligned} D_{2j}^* &= \sum_{i=0}^{j} \left[D_{j*}^{(i)} l^{2i} + D_{j*}^{(i)*} l^{2i-1} m \right] \\ D_{2j} &= \sum_{i=0}^{j} \left[D_j^{(i)} l^{2i} + D_j^{(i)*} l^{2i-1} m \right] \end{aligned} \tag{B.3}$$

with $D_{0*}^{(j)} = D_{0*}^{(j)*} = D_j^{(j)*} = 0$.

Rather than solving directly for the decomposition of Z_j in terms of K_k, the idea [26] is now to turn the problem upside down and look for the decomposition of K_k in terms of Z_j:

$$\begin{aligned} K_k &= \sum_{j=k}^{N/2-1} E_j^{(k)} \frac{Z_j}{l^{2j}} + \sum_{j=k+1}^{N/2} E_{j*}^{(k)} \frac{Z_j^*}{l^{2j-1} m} \\ K_k^* &= \sum_{j=k}^{N/2-1} E_j^{(k)*} \frac{Z_j}{l^{2j}} + \sum_{j=k}^{N/2} E_{j*}^{(k)*} \frac{Z_j^*}{l^{2j-1} m} . \end{aligned} \tag{B.4}$$

The determination of the coefficients E can be turned into a combinatorial counting problem as follows. First, recall that K_k and K_k^* were defined as *traces* over restricted states (in contradistinction to the partition function which, as we have seen in (A.2), is more complicated than just a trace). We must now determine how many times each Z_j and Z_j^* occurs within a given trace. Consider therefore some configuration $\mathcal{C}$ on the annulus that contributes to (say) Z_j (i.e., has $2j$ non contractible unblobbed

loops). An example with $j = 2$ and $N = 12$ is shown in Fig. 19a. It is convenient to not represent the contractible loops within the configuration, i.e., to depict it as a state. This configuration will contribute to the trace only over such restricted states $\mathcal{S}$ that are left *invariant* by the action of the configuration. Therefore, $\mathcal{S}$ must contain the same arcs as does $\mathcal{C}$ in its top row (see Fig. 19b). It suffices therefore to determine the parts of $\mathcal{S}$ which connect onto the starting points of the $2j$ non contractible loops (see Fig. 19c). Since the goal is to determine the contribution to (say) K_k, precisely $2k$ strings and $j - k$ arcs must be used.

With this in mind, the coefficients E are then determined as the following counting problems. In all cases, construct a reduced state on $2j$ strands, using $2k$ strings and $j - k$ arcs. Further:

- For $E_j^{(k)}$, all strings are unblobbed, but the *exterior* arcs to the left of the first string may be blobbed.
- For $E_j^{(k)*}$, the problem is the same, except that the leftmost string must be blobbed. But evidently this leads to the same counting, and so $E_j^{(k)*} = E_j^{(k)}$.
- For $E_{j*}^{(k)}$, the leftmost strand becomes blobbed (since we are considering a contribution from Z_j^*), and so must connect onto a blobbed object (arc or string). But as the strings are unblobbed (since we are considering a contribution from K_k), it follows that the leftmost object is a blobbed arc.
- For $E_{j*}^{(k)*}$, the leftmost object (arc or string) as well as the leftmost string must be blobbed.

These counting problems are easily solved using generating function techniques. As a warmup, consider the counting of restricted states made up of only arcs. Associate to each *pair* of sites an activity z. A state is either empty, or has a leftmost arc which divides the space into two parts (inside the arc and to its right) each of which can accommodate an independent arc state. The generating function $f(z)$ therefore satisfies $f(z) = 1 + z[f(z)]^2$ with regular solution

$$f(z) = \frac{1 - \sqrt{1 - 4z}}{2z} = \sum_{n=0}^{\infty} C_n \, z^n \,. \tag{B.5}$$

The coefficients are the celebrated Catalan numbers $C_n = \frac{(2n)!}{n!(n+1)!}$.

Consider next states made up of only arcs, but in which exterior arcs may (but need not) be blobbed. Call the generating function $g(z)$. If the state is non-empty, the leftmost arc is necessarily exterior. Inside it are $f(z)$ states, and to its right $g(z)$ states. Thus, $g(z) = 1 + 2zf(z)g(z)$, or

$$g(z) = \frac{1}{\sqrt{1 - 4z}} = \sum_{n=0}^{\infty} \binom{2n}{n} z^n \,. \tag{B.6}$$

We can now attack the case of $E_j^{(k)}$. Since there are $2k$ strings (all unblobbed), all of which divide the space into independent parts, the generating function reads

$$h_k(z) = g(z) \times z^k \, [f(z)]^{2k} = \sum_{n=k}^{\infty} \binom{2n}{n-k} z^n \tag{B.7}$$

and we infer that $E_j^{(k)} = E_j^{(k)*} = \binom{2j}{j-k}$.

For $E_{j*}^{(k)}$ it follows from the above observations that the generating function with $2k$ strings reads

$$i_k(z) = zf(z)h_k(z) = \sum_{n=k+1}^{\infty} \binom{2n-1}{n-k-1} z^n \tag{B.8}$$

and so $E_{j*}^{(k)} = \binom{2j-1}{j-k-1}$.

Finally, for $E^{(k)*}_{j*}$ we must distinguish between the cases where the leftmost object is an arc or a string. This gives the generating function

$$j_k(z) = (1 + zf(z)g(z))\, z^k \left[f(z)\right]^{2k} = \sum_{n=k}^{\infty} \binom{2n-1}{n-k} z^n \tag{B.9}$$

whence $E^{(k)*}_{j*} = \binom{2j-1}{j-k}$.

To summarize, we have shown that

$$\begin{aligned} K_k &= \sum_{j=k}^{N/2-1} \binom{2j}{j-k} \frac{Z_j}{l^{2j}} + \sum_{j=k+1}^{N/2} \binom{2j-1}{j-k-1} \frac{Z^*_j}{l^{2j-1}m} \\ K^*_k &= \sum_{j=k}^{N/2-1} \binom{2j}{j-k} \frac{Z_j}{l^{2j}} + \sum_{j=k}^{N/2} \binom{2j-1}{j-k} \frac{Z^*_j}{l^{2j-1}m}\,. \end{aligned} \tag{B.10}$$

It is easily checked that this system of equations is invertible, and after some straightforward manipulations the Z_j and Z^*_j can be isolated. In the notation of (B.2) the solution reads

$$\begin{aligned} D^{(j)}_k &= (-1)^{j+k} \binom{j+k}{2k}, \qquad D^{(j)}_{k*} = (-1)^{j+k-1} \binom{j+k-1}{2k-1} \\ D^{(j)*}_k &= (-1)^{j+k} \binom{j+k-1}{2k}, \qquad D^{(j)*}_{k*} = (-1)^{j+k} \binom{j+k-1}{2k-1} \end{aligned} \tag{B.11}$$

Applying (B.3) then finally leads to (3.11).

References

[1] J. Cardy, J. Stat. Phys. **125**, 1 (2006); cond-mat/0604043.

[2] M. Bauer and D. Bernard, *SLE, CFT and zig-zag probabilities*, in Proceedings of the NATO conference *Conformal invariance and random spatial processes* (Edinburg, 2003); math-ph/0401019.

[3] H. Saleur, *Lectures on non perturbative field theory and quantum impurity problems*, in *Topological aspects of low dimensional systems* (Les Houches lectures, vol. 69), p. 473 (Springer, 1999); cond-mat/9812110.

[4] V. Schomerus, Class. Quantum Grav. **19**, 5781–5847 (2002); hep-th/0209241.

[5] V. B. Petkova and J. B. Zuber, *Conformal boundary conditions and what they teach us*, hep-th/0103007.

[6] V. Schomerus, Phys. Rep. **431**, 39–86 (2006); hep-th/0509155.

[7] P. Martin and H. Saleur, Lett. Math. Phys. **30**, 189–206 (1994).

[8] P. P. Martin and D. Woodcock, J. Algebra **225**, 957 (2000); math.RT/0205263;

[9] R.J. Baxter, S.B. Kelland and F.Y. Wu, J. Phys. A: Math. Gen. **9**, 397 (1976).

[10] J.L. Cardy, J. Phys. A **25**, L201 (1992).

[11] A. Nichols, V. Rittenberg and J. de Gier, J. Stat. Mech. **0503**, P003 (2005), cond-mat/0411512; A. Nichols, J. Stat. Mech. **0601**, P003 (2006), hep-th/0509069; A. Nichols, J. Stat. Mech. **0602**, L004 (2006), hep-th/0512273.

[12] H. Saleur and M. Bauer, Nucl. Phys. B **320**, 591–624 (1989).

[13] A. Doikou and P.P. Martin, J. Phys. A **36**, 2203–2226 (2003); hep-th/0206076.

[14] N. Read and H. Saleur, Nucl. Phys. B **613**, 409 (2001); hep-th/0106124.

[15] J.L. Jacobsen and J. Salas, J. Stat. Phys. **122**, 705–760 (2006); cond-mat/0407444.

[16] B. Nienhuis, Phys. Rev. Lett. **49**, 1062–1065 (1982).

[17] I. Kostov, B. Ponsot and D. Serban, Nucl. Phys. B **683**, 309–362 (2000); hep-th/0307189.

[18] I. Kostov, private communication.

[19] V. Pasquier, J. Phys. A **20**, L1229 (1987).

[20] A. Rocha-Caridi, in S. Lepowski, S. Mandelstam and I.M. Singer (eds.), *Vertex operators in mathematics and physics*, MSRI Publications No. 3 (Springer, New York, 1985), p. 451.

[21] L.H. Kaufman and S.H. Links, *Temperley Lieb recoupling theory and invariants of three manifolds* (Princeton University Press, 1994).

[22] V. Pasquier, Comm. Math. Phys. **118**, 355 (1988).

[23] J. Rasmussen, P. Pearce and J.-B. Zuber, J. Stat. Mech. **0611** (2006) P017; hep-th/0607232.

[24] A. Y. Alekseev and V. Schomerus, Phys. Rev. D **60**, 061901 (1999); hep-th/9812193

[25] T. Creutzig, T. Quella and V. Schomerus, *New boundary conditions for the $c = -2$ system*, unpublished.

[26] J.-F. Richard and J.L. Jacobsen, Nucl. Phys. B **750**, 250–264 (2006); math-ph/0605016.